J Mater Sci (2009) 44:6764–6774
DOI 10.1007/s10853-009-3577-6

MESOSTRUCTURED MATERIALS

Organic–inorganic hybrid mesoporous monoliths for selective discrimination and sensitive removal of toxic mercury ions

Sherif A. El-Safty

Received: 30 November 2008 / Accepted: 12 May 2009 / Published online: 2 June 2009

Abstract The selective optical sensing is attracting strong interest due to the use of "low-tech" spectroscopic instrumentation to detect relevant chemical species in biological and environmental processes. Our development has focused on tailoring specific solid mesoporous monoliths to be used as highly sensitive solid sensors for simple and simultaneous naked-eye detection and removal processes of extremely toxic heavy metal ions such as mercury ions in aquatic samples. The methods are emerging to design optical disc-like sensors by the immobilisation two different organic groups; however, the first organic moiety can enhance the polarity of the inorganic mesoporous disc-like monoliths "additional agents" and the second one can act as a recognition center "probe". The latter one such as tetraphenylporphine tetrasulfonic acid (TPPS) probe led to facile handling of signal read-out with visual detection of ultra-trace concentrations of mercury ions at the same frequency as the human eye. The facile signaling was quantitatively evident using simple spectrophotometric techniques to indicate the TPPS–Hg(II) ion binding events. Control sensing assays of Hg(II) ions such as contact-time "signal response time", thickness of support-based sensor, reaction temperature, and pH were established for achieving enhanced signal response and color intensities. Based on our results, these new classes of optical cage sensors exhibited long-term stability of recognition and signaling functionalities of Hg(II) ions that in general provided extraordinary sensitivity, selectivity, reusability, and fast kinetic detection and quantification of Hg(II) ions in our environment.

S. A. El-Safty (✉)
Innovative Materials Engineering Laboratory, National Institute for Materials Science (NIMS), Sengen 1-2-1, Tsukuba, Ibaraki 305-0047, Japan
e-mail: sherif.elsafty@nims.go.jp

Introduction

The importance of monitoring and controlling of extremely toxic heavy metals such as mercury ions in aquatic samples is unquestionable. Hence, attractive means of improving monitoring of metal ion concentrations would be the use of simple, inexpensive, rapid responsive, and portable chemical sensors [1–4]. Sensors have the advantage of possessing high sensitivity and selectivity, as well as providing on-line and real-time analysis that has revolutionised the field of chemical analysis, particularly in critical care analysis of blood and serum samples [5]. Fabrication of solid-state colorimetric sensors for visual detection is much less advanced, even though colorimetric sensors can allow on-site, real time qualitative/semi-quantitative detection, without complicated analytical instruments [6–16]. Also, the solid sensors are often remarkably enhanced responses and selectivity with respect to comparable indicator or probe molecules. However, such developments in the form of compact instrumental free ion-sensors are still under research level and currently being investigated using different techniques like, modified sol–gel membranes, molecular imprinted polymers, nano-thin film techniques, etc.[13–15].

New technologies can offer totally new approaches to chemical analysis thus, pushing the limits can transform technologies into real methods and often leads to newer technologies. Porous monolithic architectures provide a very robust, open, and tunable periodic scaffold on the

nanometer scale [17–22]. Nanometer-sized materials with engineered features, including size, shape, composition, and function play a leading role for their emerging applications in diverse areas [23–25] The flexibility in controlling the 3D geometrical structures with uniformly shaped cylindrical and cage-like pores are of interest as potential catalysts and sorbents, because the 3D morphologies and cage functionalities should efficiently transport guest species in much more direct and easier diffusion to the network sites [26, 27]. Our recent efforts are being made in fabricating optical chemical nanosensors that incorporate simplicity in terms of fabrication time and low-cost materials but still retain the optical devices for specific "real world" sensing applications for toxic metal ions [28, 29].

The toxicity of mercury ions is well-known. Mercury ions are human carcinogen, and non-biodegradable, among all elements [30]. Accumulation of mercury is transmitted, largely through plants and aquatic resources, from emitting industries and natural activities, and finally bioconcentrated through the food chain. Dispersed in the environment, mercury ions undergo a series of biogeochemical transformations to toxic chemical species, thus provoking intensive researches of their biological effects on humans [30–32]. Organic mercury such as methylated mercury has unique chemical characteristics (due to the methyl group) that make it prone to bioaccumulate in animals and plants. Inorganic mercury compounds are expected to be the primary species in mine effluents [31, 32]. The bioavailability and toxicity of inorganic ionic mercury to aquatic life can be influenced by hardness parameters. Inorganic mercury is a central nervous system and renal toxicant. In contrast, methyl mercury is well-absorbed across membranes and is efficiently accumulated by biota. The primary target of methyl mercury toxicity is the central nervous system [33]. The acute toxicity thresholds for inorganic mercury (typically as $HgCl_2$) in freshwater organisms vary from approximately 5–230 μg/L in crustaceans, to 60–800 μg/L in fish. Methyl mercury accumulates in muscle tissue where it binds to sulfhydryl groups of muscle proteins. Inorganic mercury is not well-absorbed relative to the short-chain alkyl mercurials such as methyl mercury, and accumulates primarily in the liver and kidney [32, 33]. The design of high-performance adsorbents for environmental cleanup and heavy Hg(II) ion recovery has therefore attracted considerable attention [34]. Because the Hg(II) ions in various environments are at concentrations far below the detection limits of the most commonly used treatment methods [34–36], there is a growing demand worldwide to develop optical and portable chemical sensor materials for accurate and rapid detection and for selective recognition of Hg(II) pollutant species [37].

Here, we used the nano-sized monoliths (disc-like) as platform for the fabrication of Hg(II) ion optical sensor. Although, optical sensors based on cage-TPPS monoliths are used for visual detection of Hg(II) ions [26], but the grinded monoliths to fine powders (100-μm diameter particles) before use in the sensing assay may constrain the applicability of this materials as a desire strip for simple and smart detection and removal of toxic ions. The design of the Hg(II) ion optical sensors based disc-like monoliths is emerging two-step inclusion procedures via grafted-controlled surface modification of the cage disc-like monoliths with *N*-Trimethoxysilylpropyl-*N*,*N*,*N*-trimethylammonium chloride (TMAC) and then by immobilisation of TPPS probe. The organic–inorganic monolithic disc led to vastly improved methods by enabling new levels of instrument control and data processing, improving sensitivity, and adding versatility and selectivity to binding assays of Hg(II) ions. In addition, the current manuscript reported the influence of the contact-time "signal response time", thickness of support-based sensor, reaction temperature, and pH for enhanced signal response and color intensities of the sensing assays of Hg(II) ions.

Experiments

Chemicals

All materials were used as produced without further purification. Tetramethylorthosilicate (TMOS), which was used as the silica source and dodecane (C_{12}-alkane) were obtained from Sigma-Aldrich Company Ltd. (USA). Anhydrous ethanol and toluene were purchased from Wako (Japan). *N*-Trimethoxysilylpropyl-*N*,*N*,*N*-trimethylammonium chloride (TMAC) (50% methanol solution) and tetraphenylporphine tetrasulfonic acid (TPPS) were purchased from Gelest (Japan). The polyoxyethylene(10) stearyl ether (Brij 76, $C_{18}H_{37}(OCH_2CH_2)_{10}OH$, M.av = 711) was obtained from Wako Pure Chemicals Ltd. Osaka, Japan. Standard mercury (Hg^{2+}) and other metal ion concentrations were prepared from their corresponding AAS grade (1000 μg/mL) solutions. These stock solutions were procured from Wako Pure Chemicals, Japan. For pH adjustments, buffer solutions (0.2 M) of KCl–HCl, CH_3COOH–CH_3COONa, 3-morpholinopropane sulfonic acid (MOPS)–NaOH, 2-(cyclohexylamino) ethane sulfonic acid (CHES)–NaOH, and *N*-cyclohexyl-3-aminopropane sulfonic acid (CAPS)–NaOH were used. The MOPS, CHES, and CAPS were procured from Dojindo Chemicals, Japan, and the remaining from Wako Pure Chemicals, Japan.

Synthesis of cubic *Pm3n* monolithic-disc as probe carriers

Cubic *Pm3n* mesophase structures (HOM-9) were fabricated by using instant direct-templating of microemulsion

liquid crystalline phases of surfactants [38–40]. In typical conditions of the synthesis of cubic *Pm3n* disc-like monoliths, the composition mass ratio of Brij 76:C_{12}-alkane:ethanol:TMOS:HCl/H_2O was 1:0.5:0.5:2:1, respectively. Homogeneous sol–gel synthesis was achieved by mixing Brij 76/C_{12}-alkane/ethanol/TMOS in a 100-cm^3 beaker and then shaking at 50 °C for 2 min until homogeneous. The exothermic hydrolysis and condensation of TMOS occurred rapidly by addition of acidified aqueous solution of HCl (at pH = 1.3) to this homogeneous solution. The resulting an optical gel-like material was put in a graduate ingot and acquired the shape and size of the cylindrical casting vessel. To obtain centimeter-sized, crack-free, and disc-like silica translucent membranes, the materials were gently dried at room temperature for 3 h and then allowed to stand in a tightly closed ingot for 1 day to complete the drying process. After calcination at 450 °C for 6 h under normal atmosphere, the transparency of the disc-like membranes was lost due to the microcracking within the silica matrix, but their macroscopic shapes with high dimensional stability, rigidity (with stress 100 hPa), and porosity were retained by compressing under hot vacuum compressor (see Fig. 1).

Fabrication of organic–inorganic disc-like sensor

With a grafting technique, the calcined cubic *Pm3n* disc-like monoliths were firstly anchored via TMAC ligand in refluxing toluene for 24 h at 90–100 °C. The grafted materials were then washed using ethanol and methylene chloride, and dried under vacuum at 80 °C for 5 h. TG-DTA and NMR analyses indicated the presence of 20% functionalised silicon by using a TMAC agent. The immobilisation of TPPS probe molecules with silica disc-TMAC was achieved by adding aqueous solutions of the TPPS probe (4×10^{-3} mg/100 mL H_2O) to 1.0 g silica-TMAC solids gentle shaking for 24 h at room temperature. The functionalised disc-TPPS solid monoliths was thoroughly washed using deionised water several times until no elution was observed. The resulting solid sensor was dried at 60 °C for 2 h. The adsorption amounts (Q mmol g^{-1}) of the TPPS probe molecules at the saturation "equilibrium" step was determined according to this equation: $Q = (C_o - C_t)\, V/m$; where Q_t is the adsorbed amount at contact time t, V is the solution volume (L), m is the mass of HOM carriers (g), C_o and C_t are the initial concentration and the concentration at saturation time t, respectively. In general, the variation in the loading capacity (Q) of TPPS probe into disc-like monoliths was attributed to the interaction characteristics of the TPPS probes with the different thicknesses of silica disc-TMAC monoliths.

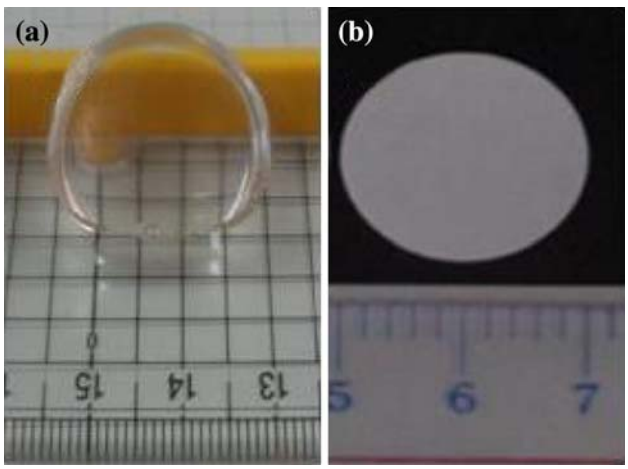

Fig. 1 **a** Transparent and **b** calcined disc-like cubic *Pm3n* mesoporous silica monoliths HOM-9 with 0.2 cm thick and 1.5 cm width that can be used as a carrier for the organic moieties

Recognition procedure for Hg(II) ions

In a typical sensing experiment, a mixture containing specific concentrations of toxic Hg(II) ions adjusted at pH solution of 9 by using CHES for the sensor. This Hg(II) analyte mixture was directly added to the monolithic sensors at constant volume (20 cm^3) with shaking at room temperature. Studies on the sample volume also indicated that the volume at 20 cm^3 was sufficient for effective interaction of Hg^{2+} with sensor disc-like strip to give good color separation. A blank solution was also prepared, following the same procedure for comparison. After an interval time of (1–5 min), the monolithic sensors were filtered after equilibration time, according to the feature of Hg(II) ion-sensors, using cellulose acetate filter paper (25 mm; Sibata filter holder) and used for visual color assessment and absorbance measurements. In a typical experiment, the Hg(II) ion-sensing system was studies by batch equilibration method at various pH values. The concentrations of toxic Hg(II) ions were calculated by comparing the color intensity of the target samples with that of the standard samples, which were prepared with known concentrations of analyte solutions.

Analyses

Small-angle powder X-ray diffraction (XRD) patterns were measured by using a 18 kW diffractometer (Bruker D8 Advance) with monochromated CuKα radiation with scattering reflections recorded for 2θ angles between 0.1° and 6.5° corresponding to d-spacings between 88.2 and 1.35 nm. N_2 adsorption–desorption isotherms were measured using a BELSORP MIN-II analyzer (JP. BEL Co. Ltd) at 77 K. The pore size distribution was then determined from the adsorption curve of the isotherms by using nonlocal density functional theory (NLDFT). Transmission

electron microscopy (TEM) was operated at 200 kV electron microscope (JEOL 2000 EX II) which has a point–point resolution of 0.21 nm and a spherical aberration of 0.7 nm. Fast Fourier Transform (FFT) patterns were recorded from by a slow scan charge-coupled device (CCD) camera (Gatan Model 694). Thermogravimetric and differential thermal analyses (TG and DTA, respectively) were done using a Thermo Plus TG8120 (Rigaku, Japan). Energy Dispersive X-ray microanalysis (EDS-130S) was used to determine the elemental compositions of the azo-probe functionalised HOM-2 carriers. ^{29}Si MAS NMR spectra at room temperature were also measured using a Bruker AMX-500 operated at 125.78 MHz with a 90^{o} pulse length of 4.7 μs. For all samples, the repetition delay was 180 s with a rotor spinning at 4 kHz. The reflectance spectra of the sensor materials were recorded by using a Shimadzu 3700 model solid-state UV–Vis spectrophotometer. The metal ion concentration after equilibration was determined with a Seiko SPS-1500 model inductively coupled plasma atomic emission spectrometer (ICP-AES). Buffer solutions were adjusted to ambient pH values using a Horiba F-24 (Kyoto, Japan) model micro-computerised pH/Ion meter.

Results and discussion

Organic–inorganic hybrid disc-like monoliths

The inclusion of (TPPS) chromophore into disc-like monolithic HOM-9 mesopore geometries led to the creation of optical chemical nanosensors that have efficient sensing functionalities (Scheme 1) in terms of sensitivity, selectivity, and response time of Hg(II) ions. Due to the potential leaching of the hydrophilic (TPPS) chromophore by the washing cycle, the TPPS probe could not be directly embedded on the silica surface matrices without tuning the surface polarity. Optical TPPS-mediated nanosensors were successfully fabricated by firstly modified TMAC-HOM silica (Scheme 1) [26, 41]. With introduction of TPPS probe molecules, strong ionic interactions successfully occurred between the TPPS chromophore containing sulfonate acid groups and the carriers charged by the functionalised ammonium ion (Scheme 1), leading to stable sensor during the sensing assays of Hg(II) ions.

^{29}Si NMR spectroscopy was used to investigate the successful immobilisation of TMAC organic and probe (TPPS) moieties through the elucidation of the molecular environment in the silica materials [42, 43]. First, ^{29}Si NMR spectrum of disc-like HOM-9 carriers (Fig. 2a) showed three overlapping signals (Q_n peaks) at −91, −101, −110 ppm, respectively [43] Second, ^{29}Si NMR spectra, for example Fig. 2b, of silica-TMAC ligand show signals representative of various silicon environments of the T_n and Q_n silane moieties; however, T_n peaks are representative of silicon matrix directly bounded to organic species. Figure 2b shows that in addition to Q_2, Q_3, and Q_4, three different signals were observed at −53, −61, −71 ppm, which correspond to three different environments for siloxane group in functionalised monolayers of T_1 [R–Si(OH)$_2$(OSi)$_3$], T_2 [R–Si (OH)(OSi)$_3$], and T_3 [R–Si(OSiO)]. This

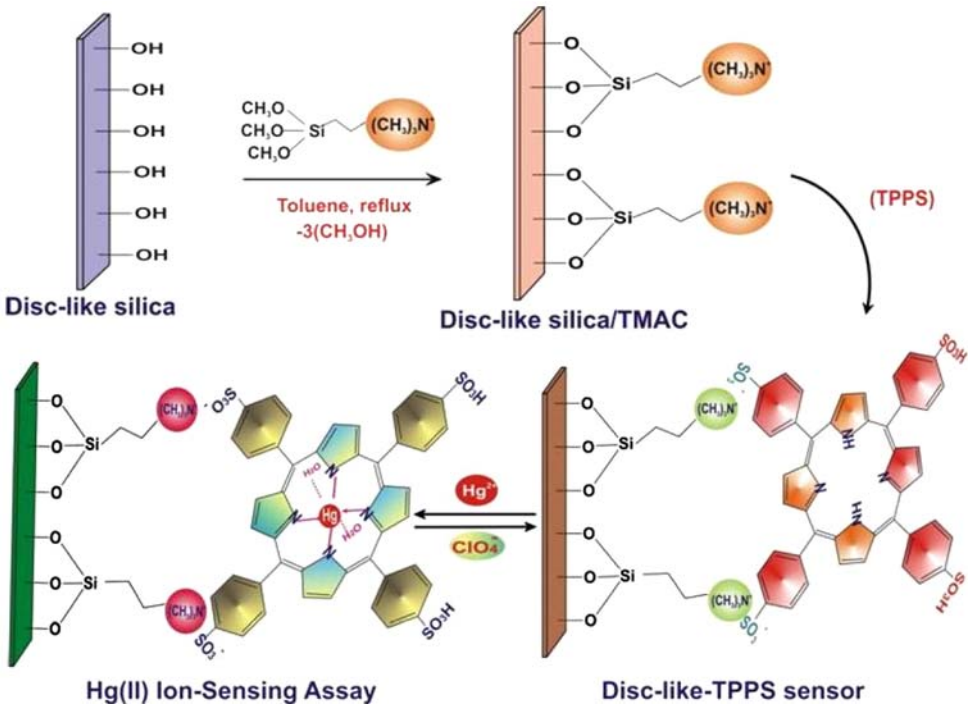

Scheme 1 Disk-like sensor for Hg(II) ion-sensing assay. The grafting technique controlled the sensor design by immobilisation of two organic moieties TMAC and TPPS into the mesopore disc-like monoliths. The reversibility of the [Hg–TPPS]$^{n+}$ complex was occurred by using of 0.01 M ClO_4^- as stripping agent for several times without leaching of the TPPS probe from the HOM pore surface

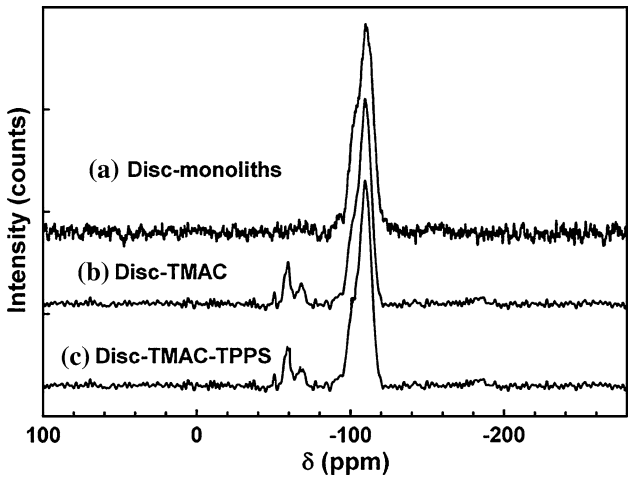

Fig. 2 ^{29}Si NMR spectra of calcined disc-like cubic *Pm3n* mesoporous silica monoliths HOM-9 (a), functionalised TMAC/HOM-9 disc-like monoliths (b), and HOM/TMAC/TPPS disc-like sensor (c)

result indicated that the silicon atom in the siloxane matrix was directly incorporated the organic TMAC moiety. The increase of the intense peak of the siloxane groups (Q_4) with the incorporation of the TMAC ligand or even TPPS indicated the Si–OH sites (silanediol and silanol groups) of the silica pore wall underwent condensation reaction with the organo-amine coupling agent, forming covalent linkage to the silica frameworks. Third, Fig. 3c shows multiple signal peaks of T_n (Fig. 2c) with the incorporation of TPPS, indicating that the TPPS molecule was loaded closely to one another in functionalised monolayer [42, 43].

Ordered organic–inorganic disc-like sensor

The XRD profiles (Fig. 3) provide evidence that the ordered primitive-centered cubic *Pm3n* structures (HOM-9) were characteristic of the fabricated disc-like monolithic carriers and nanosensors [17–20]. Despite the high loading level of the organic-probe moieties into the necked pore channels or onto the pore surface, resolved Bragg diffraction peaks were clearly evident for the cubic *Pm3n* disc-like nanosensor geometries. This finding indicated the successful immobilisation of the hydrophilic TPPS chromophore into rigid condensed framework matrices while retaining the mesoscopically orientational order (Fig. 3) of cubic *Pm3n* mesostructures. These rigid matrices with such order led to high flux and transport of Hg^{2+} analyte ions during the detection process [24–27]. Moreover, the XRD pattern (Fig. 3d) of the recovered sensors (i.e., after six regeneration/reuse cycles) revealed the diffraction peaks of cubic *Pm3n* structures. The retention of the 3D cubic structures with the disc-sensors after severe complexation/decomplexation processes of Hg(II) ions might lead to retain the Hg(II) ion-sensor assays for a long-period without significant change in the sensing functionality (see below).

The N_2 isotherms revealed uniformity and regularity of the 3D cubic cage disc-like monoliths, as evidenced from a well-known sharp inflection of adsorption/desorption branches (Fig. 4). However, H_2-type hysteresis loop and

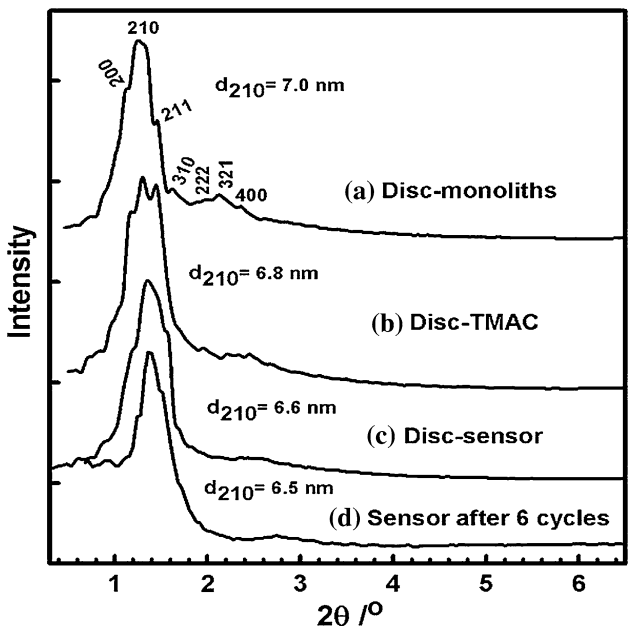

Fig. 3 The XRD diffraction patterns of calcined disc-like cubic *Pm3n* mesoporous silica monoliths HOM-9 (a), functionalised TMAC/HOM-9 disc-like monoliths (b), HOM/TMAC/TPPS disc-like sensor (c), and recovered sensor after six regeneration/reuse cycles (d). The disc-like thickness and width are 0.05 cm thick and 1.5 cm, respectively

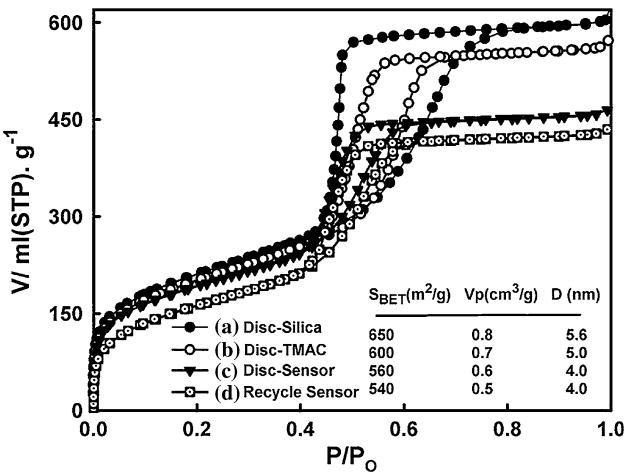

Fig. 4 The N_2 isotherms of calcined disc-like cubic *Pm3n* mesoporous silica monoliths HOM-9 (a), functionalised TMAC/HOM-9 disc-like monoliths (b), HOM/TMAC/TPPS disc-like sensor (c), and recovered sensor after six regeneration/reuse cycles (d). The disc-like thickness and width are 0.05 cm thick and 1.5 cm, respectively. Inset is the surface area (SBET), pore volume (*Vp*), and pore diameter (*D*)

well-defined steepness of isotherms (Fig. 4a) indicated that uniform cage-like pore structures were characteristic of the cubic *Pm3n* disc-like monoliths [44–46]. The adsorption branches were shifted to lower relative pressure (P/P_o) when the organic moieties (TMAC and TPPS) were immobilised (Fig. 4b, c), indicating the inclusion of the organic moieties into the spherical mesopore cavity without significant effect on the uniformly sized structures. In turn, the significant shift in desorption branches to higher relative pressure and the decrease in the width of hysteresis loop with immobilisation process of TMAC and TPPS was evident with such cage monolithic-discs. This result, in particular, is inconsistent with our previous reports using cage monoliths with large spherical cavity up to 15 nm as carrier for TPPS probe, in which no such desorption shift to higher relative pressure was observed even under the same grafting conditions [26–28]. In general, the N_2 isotherms for Disc-TMAC and Disc-TMAC–TPPS sensor (Fig. 4b, c) revealed the enlargement of cage windows under such severe grafting process (see Experiments), despite the retention of the uniformly sized cavity pores. However, the high loading of the TMAC and then TPPS into the neck of the entrance pore after partially filling of spherical cavity led to the distortion in the cage windows, as evidenced from the enlargement pore windows of the Disc-TMAC and Disc-TMAC–TPPS sensor. The latter aspect, in particular, indicated the high accessibility and retainability of the organic moieties into the entrance of the spherical cavity. From the above mentioned results, evidence of this inclusion inside the pore cavity and entrance was that, first, the width of the hysteresis loop decreased with embedding of the organic moieties, in which led to a decrease in the nanoscale pore cavity and the enlargement of the pore entrance with the fabricated nanosensor (Fig. 4b, c, inset). Second, a decrease in the surface area and pore volume with the functionalisation of cubic nanosensor provided further evidence that the organic moieties were embedded inside the mesopore. Third, with the regeneration/reuse cycles of the disc-sensor, the N_2 isotherms (Fig. 4d) revealed no change in the pore size of the cage cavity and entrance, indicating the stability of the uniformity of cage cavity and entrance. In general, the retention of physical characteristics of nanosensor; such as large porosity, surface area, and pore volume allowed the Hg^{2+} ions to access the functional active sites of the TPPS probe-based nanosensor with efficient sensing assays [44].

TEM micrographs (Fig. 5) and corresponding FTD profiles reveal well-organised mesopore arrays over a large area of the cubic *Pm3n* lattices of disc-like nanosensors, despite the immobilisation methods of the loading coverage of bulky chromophore molecules such as the TPPS probe. TEM images (Fig. 5) show uniformly sized cage-like pores and continuous spherical arrangements along all directions of the disc-like sensors [17–20], despite the slight defects, as indicated by arrows. The topological defect surfaces for these fabricated nanosensors were also

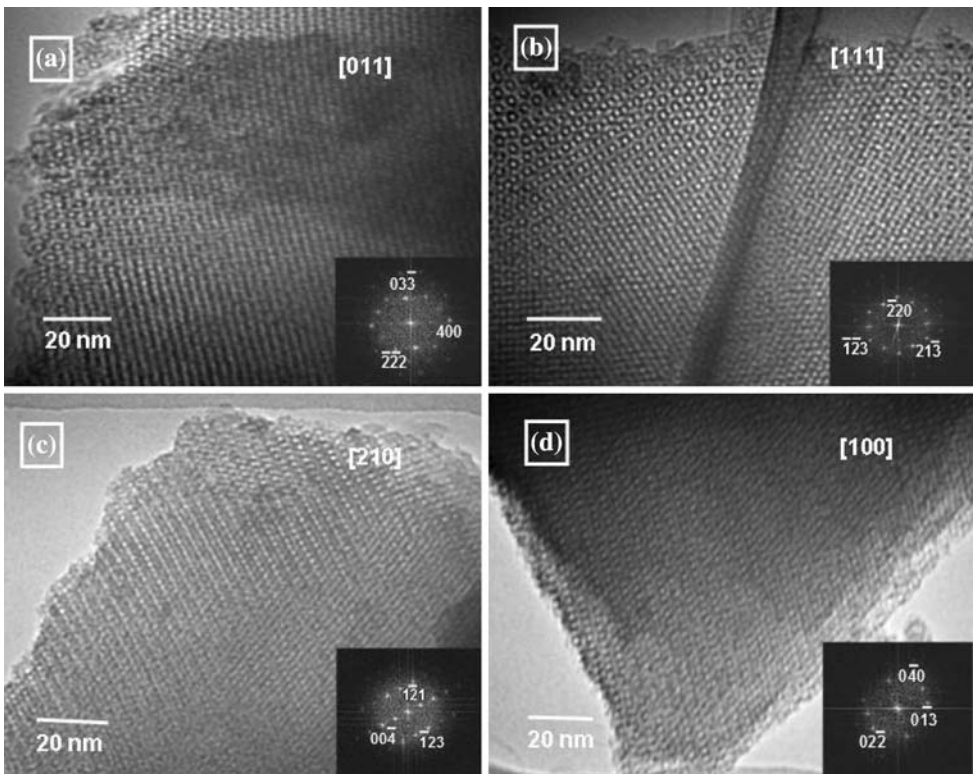

Fig. 5 Representative TEM micrographs and corresponding FTD profiles recorded along the [011] (**a**), [111] (**b**), [210] (**c**), and [100] (**d**) zone axes of ordered cubic *Pm3n* disc-like sensors (HOM–TMAC–TPPS). The FTD patterns indicated the ordered primitive-centered cubic *Pm3n* structures were attained despite the high loading coverage of TPPS probes into the pore structures

consistent with XRD patterns (Fig. 3) and N_2 isotherms (Fig. 4). In general, results indicated the retention of uniformly sized order structures with disc-like monolithic sensors, which led to facilitate the receptor-Hg(II) binding events during the sensing response assays.

Optical sensing assays of Hg(II) ions

The high performance of the sensors depended on key factors such as the contact-time "signal response time", amount of support-based sensor, reaction temperature, and pH [47–51]. In order to control the sensing assays of Hg(II) ions using disc-like sesnor, one should understand that these key factors strongly affected the homogeneity in the color map distribution and intensity even at low loading level of metal ions during the visual detection process in the laboratory experiments. In general, changes in these key factors can play significant roles involving the redistribution of the charge polarity and the electron and energy transfer within the TPPS probe molecule into the pore surfaces. Therefore, the chemical sensing system is extremely sensitive to such changes, which in turn, acutely affects the accuracy and precision in the determination and visual detection of the target ions [52].

To control sensing assays of the chemical nanosensors for Hg(II) ions ion were studied as a function of the disc-like sensor thickness, pH solution and contact-time "signal response time" (Figs. 6, 7). In this study, we carried out a series of experiments to systematically define and evaluate the relative importance of these factors in a disc-like sensor for Hg(II) ion detection. In general, the extent of the Hg(II) ion chelation with the TPPS receptor was quantitatively monitored after equilibration at real-time response (i.e., $\geq R_t$) in which the prominent color change and signal saturation of the $[Hg–TPPS]^{n+}$ complex equilibrium of binding were achieved (see Figs. 6, 7). In such quantification procedure, the response-time (R_t) can be considered as a reference signal with practically no Hg(II) analyte ion remaining. The kinetic time-response of the $[Hg–TPPS]^{n+}$ complex formation was studied by continuously monitoring the absorption spectra at λ of 450 nm (Fig. 6) and the color change of the sensors after addition of Hg(II) ion as a function of time at various sensor thicknesses. The results show that charge transfer between the Hg(II) and TPPS-probe was accomplished after 1 min. In turn, the increase of the thickness of disc-like sensor makes the Hg(II) ion-permeability through the dense TPPS probe molecular assemblies to the active binding sites more difficult. Results also indicated that the thicker disc-like sensor show difficulty in the distinguishable color changes during the detection of the trace Hg(II) ions.

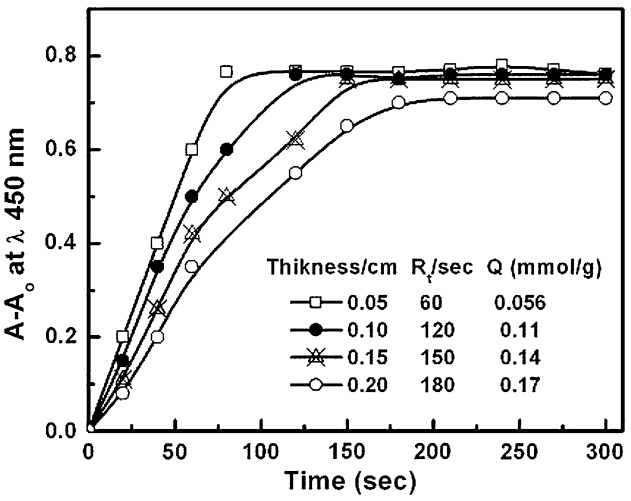

Fig. 6 Kinetic variation of the absorption signal response with respect to the thickness of disc-TPPS sesnor during the recognition of [0.6 ppm] Hg(II) ions at pH 9, at temperature 25 °C and at 25 mL of total volume. The A and A_o are the absorption signal responses of the sensor after and before (blank) the addition of Hg(II) ion

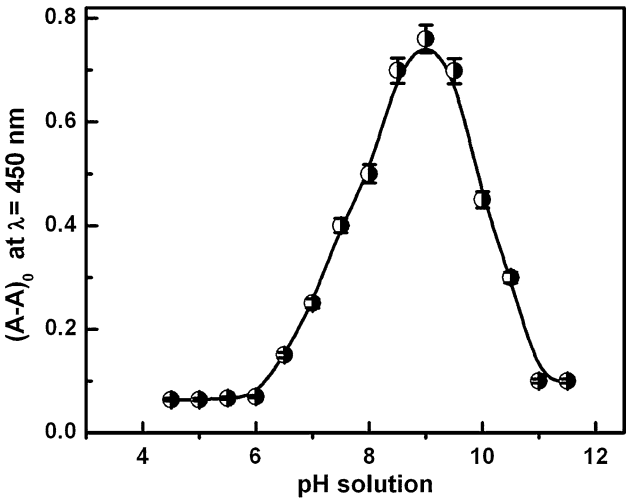

Fig. 7 pH dependent signal response of disc-TPPS sensor during the recognition of [0.6 ppm] Hg^{2+}analyte ions at λ of 450 nm. The disc thickness sensors, response time, the total volumes and temperature of the sensing systems were kept at 0.05 mg, 1 min, 25 cm^3, and 25 °C, respectively. The A and A_o are the absorption signal responses of the sensor after and before (blank) the addition of Hg(II) ion

Furthermore, the pH response was studied by continuously monitoring the signal sensing response at λ of 450 nm of the disc-like sensor for [0.5 ppm] Hg^{2+} ions at different pH solution (from 5 to 11) and at 25 °C. Note that the effect of pH on the visual detection of Hg(II) ions was studied by adding a mixture containing a specific concentration of Hg(II) ions adjusted to a pH between 4–6 (by using 0.2 M of $CH_3COOH–CH_3COONa$), 7–8 (by using 0.2 M of 3-morpholinopropane sulfonic acid, MOPS), and 8.5–11 (by using 0.2 M 2-cyclohexylamino ethane sulfonic acid, CHES), respectively (Fig. 7). Results from this pH

study showed that the maximum absorbance intensity of the $[Hg–TPPS]^{n+}$ complex exhibited at pH 9.0 (Fig. 7).

Visual detection of Hg(II) ion by disc-like sensor

Despite the feasible use of these commercial receptor TPPS probes to sensitive determination of Hg^{2+} ions up to 10^{-7} mol/dm^3 [53], our previous solid sensor-based cage cubic *Fm3m* materials immobilised by the TPPS indicator dye, in principle, showed remarkable enhancement in the sensitivity and selectivity of Hg(II) ions compared with TPPS molecular dye in solution system [26, 28, 29]. The current sensor design based on 3D inorganic scaffolds in the form of highly mechanical stable disc-like monoliths show advanced features because in addition to conventional recognition of Hg(II) ion at trace levels ($\sim 10^{-9}$ mol/dm^3) there is a further control of the sensing assay, governed by facile handling of signal read-out optical measurements. In addition, the 3D disc-like sensor could be used as simple preconcentrators to yield high adsorption capacity and preconcentration efficiency, leading to simultaneously visual inspection and complete removal of Hg(II) ions over a wide, adjustable range concentration. Moreover, still the physical properties of the 3D organic–inorganic disc-like sensor such as high surface area and porosity, and the particle-size morphology are advantageous to allow high recognition and binding of the target in sensing assay. For example, the strong binding of Hg^{2+} ions with TPPS probe onto the disc-like sensor strips led to the color change with the same frequency of the human eyes corresponding to the formation of the metal-chelate $[Hg–TPPS]^{n+}$ complex (Scheme 1). Results (Fig. 8) indicated that chemical disc-like sensors offer one-step and simple sensing procedures for both quantification and visual detection of Hg^{2+}ions without the need for sophisticated instruments under our simple sensing procedure, pH 9, temperature 25 °C, volume 25 mL, and a 0.05 cm thick. The reflectance spectra of silica disc-TPPS sensor exhibited a bathchromic shift from 410 to 450 nm during the recognition of Hg^{2+}, consistent with our previous study using similar sensor design in powder form [26]. These results indicated the formation of charge-transfer complexes between the Hg(II) ions and the TPPS probe (as shown in Scheme 1).

The calibration graphs and analytical parameters

The reflectance bands of $[Hg–TPPS]^{n+}$complex were recorded after correction of the baseline of the reflection spectra between the disc-like sensor signal of the blank and the concentration-dependent for Hg^{2+} ions at λ of 450 nm, under our simple sensing procedure, pH 9, temperature 25 °C, volume 25 mL, and a 0.05 cm thick. A linear calibration in the low level of concentration of Hg^{2+} ions with

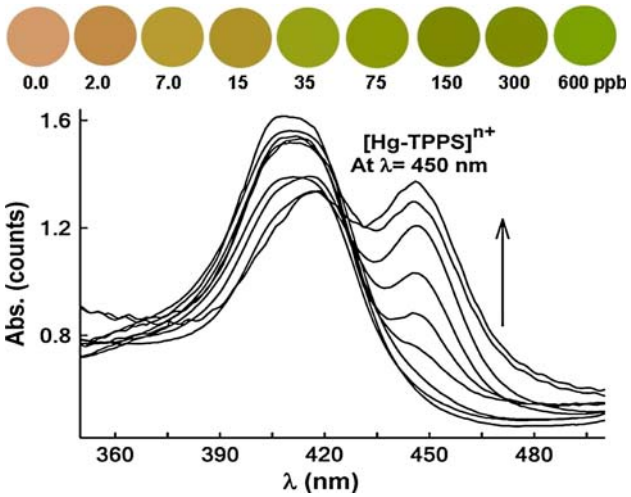

Fig. 8 Representative concentration-dependent changes of disc-TPPS sensor in the color map and in UV–Vis reflection spectra of $[Hg–TPPS]^{n+}$ complex formation at $\lambda = 450$ nm with addition of various concentrations of Hg(II) ions. The signal responses of optical sensor were monitored at specific sensing conditions (pH 9, 0.05 thick, 60 s, and 25 °C)

correlation coefficient range of $\sim$0.999 was characteristic of the calibration curve for the 3D sensor scaffolds (Fig. 9). Due to saturation effects, however, a non-linear correlation at the inflection point was observed with high concentration of Hg^{2+} ions ($\geq$0.049). The nonlinear curves indicated that the Hg^{2+} analytes can be detected with highest sensitivity at low concentrations, in agreement to our previous reports [26–29]. In fact, the quality of the calibration methods is necessary to ensure both accuracy and precision of the metal ion-sensing systems. Several quantification measurements ($\geq$10 times) were carried out over wide-range concentrations of the standard "well-known" solutions of Hg^{2+} analyte at the specific sensing conditions. The calculated standard deviation for the analysis of Hg^{2+} analyte ions using all monolithic nanosensors was of 0.4%, as evidenced form the fitting plot of the calibration graphs (Fig. 9).

The detection (L_D) and quantification (L_Q) limits of Hg(II) ions by using disc-like sensors were estimated to be 1.2 and 4.0 ppb, respectively, according to the following Eq. 1 [29]:

$$(L_D) \text{ or } (L_Q) = k\, S_b/m \qquad (1)$$

where, S_b and m are the standard deviation and the slope of the linear calibration graph (Fig. 9, inset), the constant k is equal to 3 and 10 in the case of the determination of L_D and L_Q, respectively. Furthermore, at the inflection point in the calibration curve (Fig. 9), the stoichiometry of the $[Hg–TPPS]^{n+}$ complexes was 1:1 (Hg^{II}:TPPS) (See Scheme 1). Further evidence of the stoichiometric $[Hg–TPPS]^{n+}$ complex was revealed from Job's plot (data not shown) in

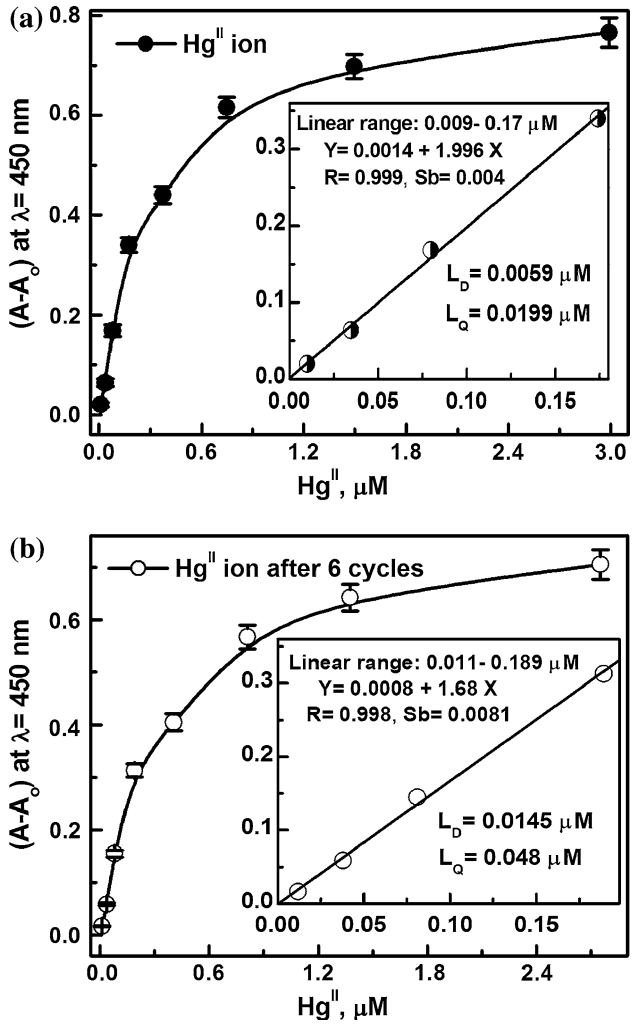

Fig. 9 Calibration curves of disc-TPPS sensor (**a**) and recovered sensor after six regeneration/reuse cycles (**b**). The plots were depicted according to the relationship between A–A_o and [Hg(II) ion] concentration, where A_o and A are the absorbance of HOM-probe (blank) of HOM–TPPS and the signal response of $[Hg–TPPS]^{n+}$ complex during the recognition of Hg^{2+} analyte ions at pH 9. The thickness of disc-like monoliths, the total volumes, and temperature of the sensing systems were kept at 0.05 thick, 25 cm^3, and 25 °C, respectively

which changes in the absorbance of the complex formation in solution under our experimental conditions (pH 9, temperature 25 °C, and volume 25 mL) were monitored. Results indicated a 1:1 binding for TPPS with Hg^{2+} ions (Scheme 1). The stability constant (log K_s) of the formed $[Hg–TPPS]^{n+}$ complex with the disc-like sensors at a specific pH value of 9.0 was estimated to be 14.8, in agreement with our previous study [26].

Reversibility of the Hg(II) ion-sensing assay

The reversibility of disc-like sensor allowed the retaining functionality in terms of sensitivity with fast response-time even after multiple regeneration/reuse cycles of the $[Hg–TPPS]^n$ complex in the solid system [26, 27]. Although the improvement of the reversibility of the chemical sensors are a challenge, the nanostructured sensor can extend control of the Hg^{2+} ion detection even after several cycles of decomplexation in which an appropriate stripping agent is used, such as 0.01 M ClO_4^- (Scheme 1). However, the disc-like sensor after removal the 0.6 ppm of Hg(II) ions was washed several times by 0.01 M ClO_4^- solution for 2 days. The released Hg(II) ion was detected by ICP-AES analysis. The gradual change in the green color to pale brown can be detected by naked eyes with increasing of the regenerated time. Moreover, the reflectance spectra of the regenerated silica-disc-TPPS solid were similar to that freshly synthesised sensor, indicating the successful removal of Hg(II) ion from the sensor without significant release of TPPS from the solid disc scaffolds. After multiple regeneration/reuse cycles (i.e., ≥6), although the regenerated disc-like sensors showed a relatively lower sensitivity up to 92% with higher Hg(II)-to-TPPS ligand kinetic hindrances (>2 min), the binding and signaling remained relatively fast, on the order of minutes, and fully revisable. It is important to note that the strong electrostatic interactions 'Coulombic-types' between the TPPS probe molecule and charged silica surfaces (i.e., disc-TMAC) led to high stability of the sensor design even with severe releasing process of Hg(II) ion by ClO_4^- anions. The reversibility of the sensor strip were quantitatively examined by measuring the Hg(II) ion signaling with the recovered sensor (Fig. 9b). Our results show that little changes in the optically colored density "absorption spectra" of probes were evident after six regeneration/reuse cycles of the $[Hg–TPPS]^n$ complex in the solid system. Although the efficiency of the recovered sensor was decreased, as shown from the L_D and L_Q values (Fig. 9b, inset), but the recovered sensor maintained the Hg(II) ion detection and removal over a wide range of concentration (2.5–550 ppb). Results for the calibration curve (Fig. 9b) indicated that the recovered sensor strip still enabled to generate and transduce an optical color signal and a fast kinetic TPPS probe-Hg(II) binding responses (in the order of minutes) even after multiple regeneration/reuse cycles.

Ion competitive sensing assay of disc-like sensor

One of the practical utility of the disc-like sensors is the ability to show high selectivity of Hg(II) ions, when combined with actively diverse ions (interfering components) under our experimental control conditions, Fig. 10. To investigate the effect of extraneous ions in the simultaneously selective detection of Hg^{2+} ions, particularly at low concentration, controlled sensing experiments

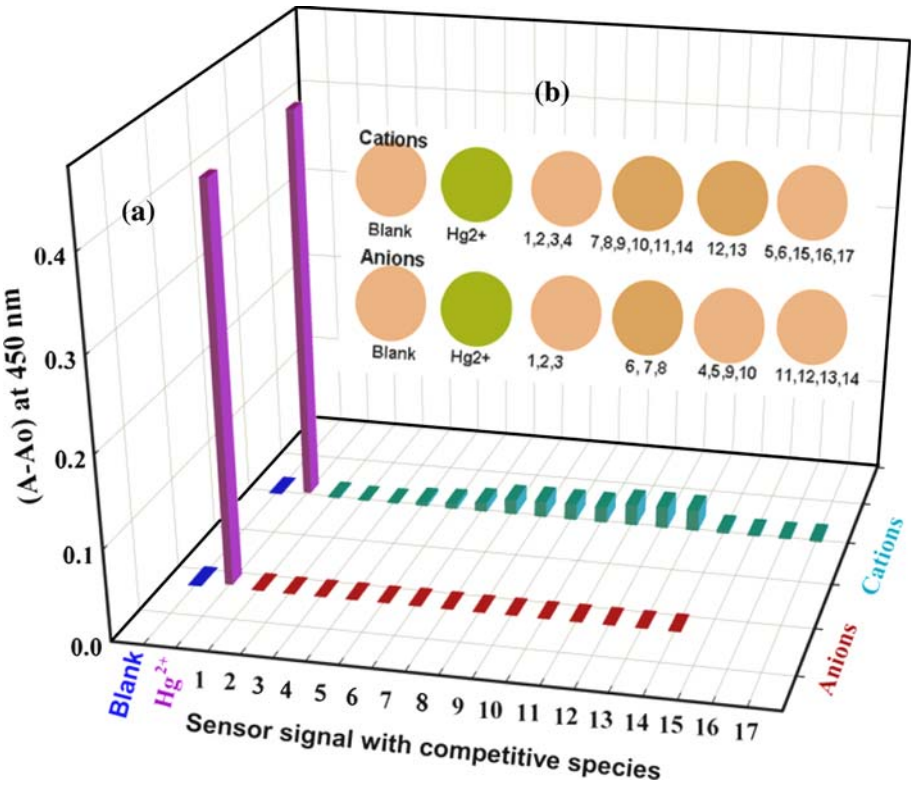

Fig. 10 Representative selectivity profiles of disc-sensor for [0.075 ppm] Hg(II) ions. The interfered cations listed in the order (*left* to *right*), (1) 6000 ppm Na^{+}, (2) 5000 ppm K^{+}, (3) 20 ppm Ca^{2+}, (4) 15 ppm Sr^{2+}, (5) 4 ppm Cr^{6+}, (6) 3.8 ppm Al^{3+}, (7) 1.5 ppm Cu^{2+}, (8) 1.8 ppm Ni^{2+}, (9) 2.5 ppm Mn^{2+}, (10) 2.2 ppm Zn^{2+}, (11) 2 ppm Co^{2+}, (12) 0.5 ppm Cd^{2+}, (13) 0.5 ppm Pb^{2+}, (14) 3.5 ppm Fe^{2+}, (15) 3.5 ppm Bi^{3+}, (16) 4.5 ppm Sn^{2+}, and (17) 4 ppm Sb^{3+}. The surfactants and anions listed in the order (*left* to *right*), (1) 10 ppm SDS, (2) 20 ppm CTAB, (3) 30 ppm Triton X-100, (4) 35 ppm tartrate, (5) 20 ppm citrate, (6) 15 ppm oxalate, (7) 300 ppm Cl^{-}, (8) 50 ppm acetate, (9) 250 ppm nitrite, (10) 32 ppm nitrate, (11) 200 ppm sulfite, (12) 255 ppm sulfate, (13) 100 ppm phosphate, and (14) 250 ppm carbonate. The selective competitive method were studied at specific sensing condition of pH 9, equilibrating time of 1 min, solution volume of 25 mL, 0.05 thick of the disc-sensor, and at 25 °C, respectively

were done here in which the competitive cations and anions were added with high concentration range of 2–6000 ppm to silica-disc-TPPS sensors (blank) at the normal sensing conditions (pH of 9, time $\geq R_t$, temperature 25 °C, volume 25 mL, and a 0.05 cm), Fig. 10. Results showed that no significant changes in reflectance spectra at $\lambda = 597$ nm and visible color patterns of sensors were observed. In turn, the addition of [0.075 ppm] Hg(II) analyte to TPPS-based disc-like sensors showed prominent color change and signal intensity (Fig. 10a, b). Results showed that no significant changes in either the developed color or the reflectance intensities were observed (Fig. 10), despite the addition of cations or anions which are effective disturbance species at higher concentrations than that of Hg(II) target ions. In fact, the selectivity of the disc-like sensors for Hg(II) ions over active multi-component ions and species (Fig. 10) indicated the high thermodynamic binding of Hg(II) ion for N-chelate TPPS ligand and the fast Hg-to-TPPS binding kinetics at the optimised pH 9.

Conclusion

The tailoring of solid mesoporous monoliths to be used as highly sensitive solid sensors for simple and simultaneous naked-eye detection and removal processes of extremely toxic heavy metal ions such as mercury ions in aquatic samples was evident. Moreover, the successful design of organic–inorganic disc-like sensor monoliths show advanced features of a further control of the sensing assay that can be governed by facile handling of signal read-out optical measurements at trace levels ($\sim 10^{-9}$ mol/dm^3) of Hg(II) ions. Results revealed that the 3D disc-like sensor could be used as simple preconcentrators to yield high adsorption capacity and preconcentration efficiency, leading to simultaneously visual inspection and complete removal of Hg(II) ions over a wide, adjustable range concentration. In addition, the disc-like sensors provided extraordinary sensitivity, selectivity, reusability, and fast kinetic detection and quantification of Hg(II) ions in the environment cleanup technology.

References

1. Miyawaki A, Lopis J, Helm R, McCaffery JM, Adams JA, Ikura M, Tsien RY (1997) Nature 388:882
2. Oehme I, Wolfbeis OS (1997) Mikrochim Acta 126:177
3. Buhlmann P, Pretsch E, Bakker E (1998) Chem Rev 98:1593
4. Keith LH, Gron LU, Young JL (2007) Chem Rev 107:2695
5. Spichiger-Keller US (1998) Chemical sensors and biosensors for medical and biological applications. Wiley-VCH, Weinheim, Germany
6. Wirnsberger G, Scott BJ, Stucky GD, Wirnsberger G (2001) Chem Commun 119
7. Nicole L, Boissiere C, Grosso D, Hesemann P, Moreau J, Sanchez C (2004) Chem Commun 2312
8. Lee SJ, Lee SS, Lee JY, Jung JH (2006) Chem Mater 18:4713
9. Palomares E, Vilar R, Green A, Durrant JR (2004) Adv Funct Mater 14:111
10. Liu J, Lu Y (2004) Chem Mater 16:3231
11. Comes M, Marcos MD, Sancenon F, Soto J, Villaescusa LA, Amoros P, Beltran D (2004) Adv Mater 16:1783
12. Capitan-Vallvey LF, Raya CC, Lopez EL, Ramos MDF (2004) Anal Chim Acta 524:365
13. Kalinina MA, Golubev NV, Raitman OA, Selector SL, Arslanov VV (2006) Sens Actuators B 114:19
14. Rodman DL, Pan H, Clarier CW, Feng W, Xue ZL (2005) Anal Chem 77:3231
15. Potyrailo AR (2006) Angew Chem Int Ed 45:702
16. Desacalzo AB, Rurack K, Weisshoff H, Mártinez-Mánez RM, Marcos MD, Amoros P, Hoffmann K, Soto J (2005) J Am Chem Soc 127:184
17. El-Safty SA, Hanaoka T (2004) Chem Mater 16:384
18. El-Safty SA, Evans J (2002) J Mater Chem 12:117
19. El-Safty SA, Hanaoka T (2003) Adv Mater 15:1893
20. El-Safty SA, Hanaoka T (2003) Chem Mater 15:2892
21. Melosh NA, Lipic P, Bates FS, Wudl F, Stucky GD, Fredrickson CH, Chmelka BF (1999) Macromolecules 32:4332
22. Melosh NA, Davidson P, Feng P, Pin DJ, Chmelka BF (2000) J Am Chem Soc 122:823
23. Lu Y, Yang Y, Sellinger A, Lu M, Huang J, Fan H, Haddad R, Lopez G, Burns AR, Sasaki DY, Shelnutt J, Brinker CJ (2001) Nature 410:913
24. El-Safty SA (2008) J Colloid Interface Sci 319:477
25. El-Safty SA, Kiyozumi Y, Hanaoka T, Muzukami F (2008) Appl Catal A 337:121
26. El-Safty SA, Balaji T, Matsunaga H, Hanaoka T, Muzukami F (2006) Angew Chem Int Ed 45:7202
27. El-Safty SA, Prabhakaran D, Ismail AA, Matsunaga H, Muzukami F (2007) Adv Funct Mater 17:3731
28. El-Safty SA, Prabhakaran D, Ismail AA, Matsunaga H, Muzukami F (2008) Chem Mater 20:2644
29. El-Safty SA, Ismail AA, Matsunaga H, Muzukami F (2008) J Phys Chem C 112:4825
30. Benounis M, Jaffrezic-Renault N, Halouani H, Lamartine R, Dumazet-Bonnamour I (2006) Mater Sci Eng C 26:364
31. Harris HH, Pickering I, George GN (2003) Science 301:1203
32. Tag K, Riedel K, Bauer HJ, Hanke G, Baronian KHR, Kunze G (2007) Sens Actuators B 122:403
33. Kaiser G, Tolg G (1980) The handbook of environmental chemistry, vol 3, part A. Springer-Verlag, NY, pp 1–58
34. Feng X, Fryxell GE, Wang L-Q, Kim AY, Liu J, Kemner KM (1997) Science 276:92
35. Metivier R, Leray I, Lebeau BD, Valeur B (2005) J Mater Chem 15:2965
36. Balaji T, Sasidrharan M, Matsunaga H (2005) Analyst 130:1162
37. El-Safty SA, Prabhakaran D, Kiyozumi Y, Mizukami F (2008) Adv Funct Mater 18:1739
38. El-Safty SA, Hanaoka T, Mizukami F (2005) Adv Mater 17:47–53
39. El-Safty SA, Hanaoka T, Mizukami F (2006) Acta Mater 54:899
40. El-Safty SA, Kiyozumi Y, Hanaoka T, Mizukami F (2008) J Phys Chem 112:5476
41. Liu AM, Hidajat K, Kawi S, Zhao DY (2000) Chem Commun 1145
42. Engelhardt G, Michel D (1987) High resolution solid-state NMR of silicates and zeolites. John Wiely and Sons, New York
43. Liu Y-H, Lin H-P, Mou C-H (2004) Langmuir 20:3231
44. El-Safty SA, Mizukami F, Hanaoka T (2005) J Phys Chem B 109:9255
45. El-Safty SA, Hanaoka T, Mizukami F (2005) Chem Mater 17:3137
46. Kruk M, Jaroniec M (2003) Chem Mater 15:2942
47. Coronado E, Galán-Mascarós JR, Martí-Gastaldo C, Palomares E, Durrant JR, Vilar R, Gratzel M, Nazeeruddin MdK (2005) J Am Chem Soc 127:12351
48. Han MS, Kim DH (2002) Angew Chem Int Ed 41:3809
49. Miyaji H, Sato W, Sessler JL (2000) Angew Chem Int Ed 39:1777
50. Rex M, Hernandez FE, Campiglia AD (2006) Anal Chem 78:445
51. El-Safty SA, Ismail AA, Matsunaga H, Muzukami F (2007) Chem Eur J 13:9245
52. Liu J, Lu Y (2004) J Am Chem Soc 126:12298
53. Sandell EB (1959) Colorimetric determination of traces of metals, 3rd edn. Interscience Publisher INC, NY